Edinburgh Research Explorer

Anatomy and histomorphology of the flexor digitorum profundus enthesis

OPEN ACCESS

1   **Anatomy and histomorphology of the flexor digitorum profundus enthesis: Functional**

2   **implications for tissue engineering and surgery**

3

4   Jeremy W. Mortimer, BMedSci (Hons), MSc, PhD, BMBS, MRCS[1]

5   jeremymortimer@doctors.org.uk

6   Hamad Alsaykhan, MBBS, MRes, PhD[1] halsaykhan@gmail.com

7   Subashan Vadibeler[1] subashan@siswa.um.edu.my

8   Philippa A. Rust, MBBS, MD, FRCS (Tr & Orth), DipHandSurg, MFSTEd[1,2]

9   philippa.rust@nhslothian.scot.nhs.uk

10   Jennifer Z. Paxton, BSc (Hons), MSc, PhD, FAS[1] j.z.paxton@ed.ac.uk

11   [1]Anatomy@Edinburgh, Deanery of Biomedical Sciences, University of Edinburgh,

12   Edinburgh, United Kingdom

13   [2]Hooper Hand Unit, St John's Hospital, Livingston, Edinburgh, United Kingdom

14

15   **Corresponding author;** Jennifer Z. Paxton, Bsc Hons), MSc, PhD, FAS

16   Anatomy@Edinburgh

17   Deanery of Biomedical Sciences

18   University of Edinburgh

19   Old Medical School

20   Teviot Place

21   Edinburgh

22   EH8 9AG

23

24   **Running title**

25   FDP enthesis anatomy and histomorphology

1 **Abstract**

2 **Background:** The enthesis possesses morphological adaptations across the soft-hard tissue

3 junction which are not fully restored during surgical avulsion repairs. This loss of anatomical

4 structure, highly related to function, contributes to poor clinical outcomes. Investigating the

5 native macro- and micro-structure of a specific enthesis can provide functional and

6 biomechanical insights to develop specialised, novel tissue-engineered therapeutic options

7 and potentially improve current surgical treatments for avulsion injuries.

8 **Methods:** This study examines the anatomy and histomorphology of the flexor digitorum

9 profundus (FDP) enthesis in 96 fresh-frozen human cadaveric fingers, quantitatively and

10 qualitatively analyzing the shape, size, angle of tendon fibres and histological architecture,

11 and explores differences in sex, finger and distance along the enthesis using linear mixed

12 effects models.

13 **Results:** Macroscopically, results showed a consistent trapezoidal insertion shape of $29.29 \pm$

14 $2.35mm^2$ mean surface area, but with significant morphometric size differences influenced

15 primarily by the smaller dimensions of the little finger. Microscopically, a fibrocartilaginous

16 enthesis was apparent with a $30.05 \pm 0.72°$ mean angle of inserting tendon fibres, although

17 regional variation in fibrocartilage and the angle change of tendon fibres before insertion

18 existed.

19 **Conclusions:** The implication of these findings on native and specific FDP enthesis function

20 is discussed whilst providing recommendations for optimal FDP enthesis recreation for

21 interfacial tissue engineers and hand surgeons. The study emphasizes the importance of

22 region-specific knowledge whilst also describing methods applicable to assessing any soft

23 tissue insertion.

24 **Key Words**

25 Flexor digitorum profundus; enthesis; anatomy; histology; interfacial tissue engineering.

1 BACKGROUND

The flexor digitorum profundus (FDP) tendon inserts into the base of the distal phalanx (DP) in the finger, functioning to provide a full fist for power grip and fingertip pinch required for everyday manual tasks. FDP avulsion from this insertion ('jersey finger') is a common, distinct clinical injury[1,2] and is the most frequent type of closed flexor tendon injury.[3-5] Such injuries have an extensive economic and social impact, both for the individual and society, due to reliance on effective manual function for work and daily living.[6,7] Multiple surgical techniques are employed to restore the FDP tendon-bone interface, primarily based on pull-out suture or bone anchor methods, but are at risk of complications such as infection, nailplate deformity, osteolysis and injurious anchor placement,[8] contributing to poor functional outcomes.[1,9,10] Furthermore, serious infective complications or complete mechanical failure of the reattachment technique require a tendon graft to restore function, with additional patient morbidity and cost. By advancing morphological understanding of the FDP insertion, both the efficacy of current techniques can be increased and new therapeutic options developed using novel tissue-engineered techniques.

The enthesis is the region of soft tissue (e.g. tendon) attachment to bone, allowing transmission of tensile force whilst providing anchorage and dissipation of stress forces between biomechanically distinct tissues.[11-13] Macroscopically, tendons flare out at their insertions, demonstrating the importance of size of interfacial surface area contact for strong attachment and stress dispersal.[12,14] Microscopically, the majority of entheses also possess an interfacial fibrocartilage transition, providing a gradation in tissue properties.[15,16] Such entheses are categorized as 'fibrocartilaginous' and encompass 4 distinct tissue zones: dense fibrous connective tissue, uncalcified fibrocartilage (UF), calcified fibrocartilage (CF), and

bone;[17-19] 'fibrous' entheses lack fibrocartilage. Surgical reattachment of an avulsed tendon does not recapitulate the fibrocartilaginous transition zone,[20-23] leaving a biomechanically inferior interface[20,22,24] that promotes re-rupture risk and poor outcome.

An important structural and biomechanical consideration at the enthesis is tendon fibre angle. A more acute attachment angle increases strain concentration at the enthesis[25] and the change in tendon fibre angle during functional tendon-bone movement generates compressive and shear forces.[18] The fibrocartilaginous enthesis has indeed been portrayed as an adaptation to counter these forces,[18] with the quantity of UF associated with a large degree of movement of inserting tendon fibres.[18,26-28] Therefore, knowledge of tendon fibre orientation at the FDP enthesis may provide biomechanical insights into function and failure, and enhance the surgical recreation, or indeed *in vitro* formation, of this native anatomical structure.

Interfacial tissue engineering (ITE) aims to establish connecting interfaces between distinct tissues *in vitro*, and has great potential to provide novel, enhanced therapeutic options for avulsion injuries such as at the FDP insertion described above. By pre-forming a replica enthesis, a surgically implanted model requires integration of only homogenous engineered and native tendon and bone tissue, rather than the heterogenous structures at the complex but vital interface. To realise translational potential, ITE must be specific to a body region, and development of an ITE FDP model demands detailed understanding of FDP enthesis macro- and micro-anatomy. The human FDP enthesis has received little attention, particularly compared to entheses around large joints. Studies regarding its insertional anatomy are limited to position on the DP[29] and vasculature,[30] whilst histologically it is mentioned only as part of broad surveys of numerous enthesis sites.[31-34] This study therefore addresses the FDP

enthesis anatomy crucial to designing a clinically relevant ITE model, using techniques applicable to any enthesis.

The overall aim of this study was to analyze the FDP enthesis in macroscopic and microscopic detail, focusing on shape, size, and tendon fibre angle. The specific aims were to: 1) gain insight into biomechanical functionality, 2) aid translational ITE design, and 3) enhance knowledge relevant to current surgical repair techniques of the avulsed tendon. Both qualitative and quantitative analyses were performed, with morphometric variation explored through comparison of different sexes, fingers and distances along the enthesis.

2 METHODS

2.1 Tissue Procurement and Dissection

A retrospective cohort study of type III evidence was performed on fresh-frozen human cadaveric tissue, obtained from The University of Edinburgh Medical School body donation programme and regulated by The Human Tissue (Scotland) Act (2006). All donors consented to photography before death.

All 96 fingers from 12 donors were dissected for either footprint (3 male donors, 3 female; mean age 82.2, range 65 - 95) or histological (3 male, 3 female; mean age 79.3, range 73 - 91) investigation, selected as a sample of convenience but to provide equal sex balance. 3x magnification was used throughout dissection, and no gross pathology or previous surgery of the FDP insertion was observed. Fingers from both study groups underwent the same initial dissection to obtain an isolated FDP-DP tendon-bone sample: from a midline flexor

approach, all appreciable soft tissue was sharply removed from the DP except for an

approximate 5cm length of FDP. All components of the distal interphalangeal joint (DIPJ)

capsule were carefully excised with avoidance of FDP insertion disruption.

2.2 Insertion Footprint Analysis

Shape and size of the FDP insertion were assessed by revealing the tendon footprint on the

bone, adapting and enhancing a previously published inking methodology.[29] The isolated

FDP-DP sample was immersed in methylene blue 1% w/v aqueous solution (Scientific

Laboratory Supplies Ltd, Coatbridge, UK) for 10 seconds, and excess ink briefly blotted

away on removal (**Figure 1a, b**). The FDP was then sharply dissected away at the bone-

tendon interface, leaving the unstained FDP footprint (**Figure 1c**). After drying at room

temperature (1 hour), a digital photograph of the unstained FDP footprint was captured for 2-

dimensional (2-D) image measurements. During optimisation of the inking timeframe, one

sample underwent 90 minute immersion, noticeably reducing the footprint size, and was

therefore excluded from further analysis, leaving a sample size of 47 footprint images.

Image analysis of digital photographs was conducted using ImageJ software (National

Institutes of Health, Bethesda, MD). The FDP footprint perimeter was manually outlined at

the demarcation of peripheral colour change, at the point where variation from the dark blue

of the methylene blue was first perceived, and subsequently processed into a binary mask

image (**Figure 1d**). Footprint surface area was calculated from the mask image, whilst a

software-generated bounding box applied to the mask image perimeter allowed precise

measurements of the height, base width, apex width and 4 principal internal angles of the

1   footprint shape (**Figure S1**). A 2nd observer undertook all footprint measurements on the

2   original unprocessed photographs using the same image analysis technique.

3

4   **2.3 Histological Analysis**

5

6   Isolated tendon-bone samples for histological observation were further trimmed by excision

7   of their ungual tuberosities and shortening of the attached FDP to approximately 5mm.

8   Samples were immediately fixed in 10% neutral buffered formalin (Merck Life Science,

9   Gillingham, UK) for 48 hours at 4°C, then decalcified in Decalcifying Solution-Lite (Merck

10   Life Science, Gillingham, UK) for 72 hours at room temperature with gentle rocking and 24

11   hour solution changes. Decalcified samples underwent standard machine processing and

12   manual embedding in paraffin wax, following which para-sagittal 10µm sections were cut to

13   the longitudinal axis and floated onto standard glass slides, dried at 37°C before staining.

14   Sections were collected across the central 800µm in the mid-sagittal plane of the enthesis,

15   calculated using pre-analyzed data of the mean FDP footprint base width for a particular

16   finger and sex. Sections were stained in haematoxylin and eosin (H+E) (qualitative overview

17   analysis) and 0.1% toluidine blue (qualitative and quantitative analysis), and high resolution

18   images of entire sections acquired using a Nanozoomer XR slide scanner (Hamamatsu,

19   Welwyn Garden City, UK).

20

21   Qualitative analysis examined sections for tissue structure and overall configuration of

22   tendon fibres at the enthesis. Quantitative tendon fibre angle measurements were performed

23   on a single toluidine blue stained section on one slide per tendon-bone sample, selected by

24   random number generation. One slide was discovered to contain crumpled sections not

25   allowing representative assessment of tendon fibre angles, and after its exclusion the

remaining sample size for quantitative analysis numbered 47 entheses. Angle measurements

were performed adapting a previously published method using Image J,[25,35] defining the

angle situated between a line parallel with the FDP tendon fibres and a line of best fit of the

enthesis tidemark. Both the angle of fibres intersecting the tidemark (*'inserting fibres'*) and

fibres running over a preceding 20% length of the enthesis before reaching the tidemark

(*'approaching fibres'*) were measured at 5 enthesis distance points (20%, 40%, 50%, 60%

and 80% along the proximal-distal length) (**Figure 2**). '*Angle change*' was defined as the

difference in angle between approaching and inserting fibres. All angle measurements were

repeated by a 2nd observer on the original blank section images using the same methodology.

2.4 Statistical Analysis

Statistical tests were performed in SPSS (version 24; IBM, Armonk, NY). Linear mixed

effects models were employed to account for correlation of samples from the fingers of the

same donor, where donor identification was defined as a random effect and output generated

estimated marginal means and standard errors in all models. A series of models tested

hypotheses of the size effect of different sex, finger and individual finger (classified by both

sex and finger), as fixed factors testing main effects, for both footprint and tendon fibre angle

analysis. Further models tested side of base and apex internal footprint angle and enthesis

distance measurement point as additional fixed factors, for footprint shape and tendon fibre

angle analysis, respectively. An alpha level of 0.05 was set, and a Bonferroni post-hoc

correction applied. Reliability of measurements was ascertained by the intraclass correlation

coefficient (ICC) of single measures of absolute agreement between the 2 observers,

presented with 95% confidence intervals.

3 RESULTS

3.1 FDP Footprint Morphometrics

The FDP insertion footprint was a consistent shape, approximately trapezoidal and almost triangular (**Figure 3a**). A flat, wide base narrowed distally to a more variable flat or rounded apex. Left and right internal trapezoid angles were similar, implying a symmetrical footprint shape (**Figure 3b**, **Table S-1**). Overall mean surface area of insertion was $29.29 \pm 2.35 \text{mm}^2$. As an indication of general size differences, surface area ranged from the female little finger ($19.50 \pm 3.56 \text{mm}^2$) to male middle ($39.11 \pm 3.56 \text{mm}^2$), with little finger surface area significantly smaller than all other fingers both with sexes combined (index, $p < 0.01$; middle and ring, $p < 0.001$) and within males (index and ring, $p < 0.01$; middle, $p < 0.001$), and significantly smaller than the middle finger within females ($p < 0.05$) (**Figure 3c**). ICCs for internal angle and surface area measurements were 0.99 (0.990 – 0.993) and 0.97 (0.95 – 0.98), respectively.

Overall mean height, base width and apex width of the footprint were $5.45 \pm 0.21 \text{mm}$, $8.58 \pm 0.37 \text{mm}$, and $1.60 \pm 0.11 \text{mm}$, respectively, with individual finger means and combined means for sex and finger reported in **Table 1**. For height measurements [ICC 0.81 (0.72 – 0.87)], the little finger was significantly shorter than all other fingers for both combined sex (all $p < 0.001$) and within males (index, $p < 0.01$; middle, $p < 0.001$; ring, $p < 0.05$), with females also significantly shorter than males overall ($p < 0.05$). For base width [ICC 0.85 (0.74 – 0.91)], the little finger was significantly narrower than middle ($p < 0.001$) and ring fingers ($p < 0.05$), with the index also significantly narrower than the middle ($p < 0.05$), for combined sex, and within males the little finger was significantly narrower than the middle (p

< 0.05). No significant differences were found for apex width [ICC 0.40 (0.04 – 0.65)] between or within finger or sex groupings.

3.2 Qualitative Histomorphology

The FDP enthesis could be classified as fibrocartilaginous, as a fibrocartilage transition between the FDP tendon and DP bone was apparent in all samples (**Figure 4**). The fibrocartilage transition was not, however, present throughout the entire enthesis. Considerable enthesis regions contained no fibrocartilage at all, indicating localized fibrous insertion, with some regions possessing only CF without UF. Fibrocartilage, especially UF, predominated in the proximal enthesis region towards the DIPJ (**Figure 5b**), becoming less substantial and more sporadic or absent distally (**Figure 5c** and **d**).

The enthesis tidemark commenced as a prolongation of the DIPJ volar plate tidemark and continued distally either between UF and CF zones, or tendon and CF when no UF intervened, and merged with the tendon-bone junction in fibrous regions without fibrocartilage. The dense collagen fibre bundles of the tendon were straight when nearing the tidemark where little or no preceding UF was present (**Figure 5c** and **d**), but curved when traversing regions of abundant UF (**Figure 5b**). Tendon fibres did not appreciably deviate as they crossed through the CF zone, maintaining the same angle at the tidemark as at the tendon-bone junction (**Figure 4**).

3.3 Quantitative Histomorphology

Tendon fibre angle could be measured at 71.91% and 83.40% of distance measurement points across all quantitatively analysed sample sections, for inserting and approaching fibres, respectively. Exclusions were made due to cortical bone loss, haphazard degenerated fibres or poor fibre definition, preventing accurate or reliable assessment. ICCs were 0.91 (0.87 – 0.93) for all angle measurements made, 0.82 (0.75 – 0.87) for intersecting fibres and 0.80 (0.74 – 0.84) for approaching fibres, and, for separate distance measurement points, ranged from 0.86 (0.78 – 0.91) at the 40% point to 0.94 (0.90 – 0.96) at the 20% point.

The overall mean angle of inserting fibres was $30.05 \pm 0.72°$. Averaged across all enthesis distance measurement points (**Table 2**), there were no significant differences between individual fingers, or fingers of combined sexes, although a significant difference of 4.55° ($p < 0.05$) was present between sexes. Inserting fibre angles were similar across all distance measurement points, ranging from $27.69 \pm 1.51°$ (80% point) to $33.05 \pm 1.47°$ (40% point) for overall data (all measurements reported in **Table S-2**), with no significant difference existing between distance points within finger or sex groupings. The angle of approaching fibres averaged 15.20° overall, and all measurements (reported in **Table S-3**) were more acute than their inserting fibre counterpart, describing a widening of angle as fibres came to insert. This angle change exhibited significant variability along the enthesis length. The greatest angle change was present at the 20% enthesis distance point ($21.05 \pm 1.47°$) significantly wider than the angle change at the 50%, 60% and 80% points by 8.41° ($p < 0.001$), 9.21° ($p < 0.001$) and 7.34° ($p < 0.01$), respectively, for overall data (**Figure 5e**).

4 DISCUSSION

FDP avulsion injury incurs considerable functional morbidity and outcomes after surgical repair are often poor.[1,8-10] The enthesis at the tendon-bone interface is naturally designed with adaptations for optimum function and damage prevention, not satisfactorily restored through current surgical methods. This study has examined key structural features of the native enthesis as a guide to developing a novel tissue engineered replacement and to potentially enhance current surgical techniques. Results revealed a consistent trapezoidal insertion shape, with significant size differences primarily influenced by smaller little finger dimensions, and a fibrocartilaginous enthesis with uniform inserting tendon fibre angle but regional variation in fibrocartilage content and change in tendon fibre angle. The implications of these findings on biomechanics, ITE design and surgical repair are considered within their macroscopic and microscopic context.

Macroscopically, the consistency of the trapezoidal insertion suggests biomechanical advantages to the shape. The FDP insertion is at risk of avulsion due to a powerful muscle belly combined with narrow attachments to effect strong but precise movement. The distal FDP tendon has a flattened oval shape in cross section, but flaring out to a trapezoidal insertion fills the wide base and narrowing proximal shaft on the DP flexor surface, maximising tendon-bone contact surface area to spread stress force whilst retaining function-specific positioning. Repetition of this insertion shape over all fingers, as well as acting as a further avulsion risk reducing mechanism by distributing muscle force over multiple tendon attachments,[13] implies that the shape also favourably balances increased surface area with minimal areas of stress concentration. Recreation of the trapezoidal interface shape should therefore be a key aim for ITE design and surgical repairs.

1 A strong repair of a trapezoidal insertion may be achieved by 3 point fixation: 2 at the

2 insertion base and 1 at the apex. Such an arrangement for an FDP repair can be fashioned

3 with 2 micro bone anchors at the insertion base corners and a pull-out suture at the apex,

4 favoured by certain authors as a strong and reliable repair.[2,36] Although some surgeons may

5 consider that this technique increases technical complexity and potential for complications, it

6 optimally reconstructs an important morphological and biomechanical feature, as well as

7 providing an ultimate tensile strength similar to the native insertion.[36] For tissue engineers,

8 the challenge is to construct and maintain the trapezoidal interface, between engineered

9 tendon and bone components which may be of either fixed or variable form during *in vitro*

10 culture. Fixed form scaffolds (e.g. bone ceramics) require precise fabrication to achieve the

11 specific interface area, whilst scaffolds varying in shape during culture (e.g. contracting

12 hydrogels) may need morphological manipulation. Formation and culture using either

13 scaffold type demands detailed design specifications, for example for 3-D printed molds,

14 culture well inserts or bioreactors, based on the morphometric footprint data in **Table 1**.

15

16 **Table 1** serves as a size guide for constructing the trapezoidal FDP insertion, for a single

17 average size or multiple sizes based on a particular sex and finger. Surgically this information

18 may be especially valuable in chronic, neglected avulsions or complex revisions demanding a

19 tendon graft and no DP footprint haematoma is visible. The significant size variability for

20 height and base width dimensions indicates that a universal size approach may not be

21 appropriate surgically or for translatable ITE designs. Equally, 8 different sizes differing by

22 fractions of millimetres is not practical or resourceful. When considering meaningful size

23 differences, the major trends in significantly different data may provide the best approach.

24 With all but 1 significant size differences between fingers involving the little finger (surface

25 area, height, base width), the little finger alone might be categorized as one size level lower.

Due to smaller female dimensions compared to males [surface area, height (significantly), base width] it may also be appropriate to group the lower level male size (little finger) with the higher level female size (index, middle, ring finger) as their means are also similar. The lower level female size (little finger) then stands as a separate category. Averaging data in **Table 1** within these categories to the nearest millimetre establishes a 3-level size guide (**Table 3**) that may optimally balance variability with practicality, based on pragmatic whole millimetre designs.

Microscopically, the fibrocartilaginous nature of the FDP enthesis was confirmed. This classification was expected due to the FDP insertion position, near the DIPJ, since attachment to bony epiphyses and apophyses is characteristic of fibrocartilaginous entheses.[13,19,37] Tendon fibres of fibrocartilaginous entheses are classically described as crossing the tidemark at approximate right angles,[11,37,38] whereas fibres in areas lacking fibrocartilage attach to bone at acute angles.[37] The finding that inserting FDP fibres, measured intersecting the tidemark, averaged $30.05 \pm 0.72°$ aligns with the observation that, although classified as fibrocartilaginous overall, substantial areas of the enthesis lacked distinguishable fibrocartilage and were fibrous.

Fibrocartilage appeared to predominate in the proximal enthesis region, agreeing with previous histological reports of fibrocartilage concentrated in the tendon portion nearest the joint it crosses.[37,39] Furthermore, the tendon fibre angle change was significantly widest at the most proximal enthesis distance point measured (20% length), implying that this proximal region is of particular biomechanical importance. UF presence mitigates against the shear force produced by these proximal fibres undergoing a wider angle change before insertion by promoting gradual fibre bending.[11,18,26-28] UF in particular also protects against compression

forces,[12,18,40] demonstrating likely compression of the more proximal (deeper) FDP fibres by more distal (superficial) fibres during DIPJ movement. CF relates to the degree of tendon loading on the bone,[18,26,27] suggesting greater force transmission through these proximal/deeper tendon fibres, which may also explain the frequent finding of a convex bony profile at the enthesis, with peak elevation inclined more proximally, deformed by the more proximal fibres. Investigation of whether chronic degeneration or acute avulsion begins more or less frequently in the proximal region would divulge the level of protection afforded by the fibrocartilage in this vulnerable area.

The foremost implications on FDP ITE design and surgical avulsion repair from the microscopic findings are establishing a fibrocartilaginous interface with an overall approximate insertion angle of 30°. Since the fibrocartilaginous tissue zones are not regenerated in surgical repair[20-23] this confirms the importance of ITE research at the FDP insertion, both for *in vivo* repair augmentation and *in vitro* models. Promising *in vivo* studies promoting fibrocartilage formation and mechanical properties at repair sites, for example with cellular therapy or biochemical modulation, remain primarily in the animal model stage[41,42] whilst *in vitro* models are not morphologically specific to a particular enthesis. Before employing strategies to establish the fibrocartilage transition, throughout the entire interface or regionally, enthesis specificity can be enhanced by recreating the native tendon fibre insertion angle, and consequently the local biomechanics. For an FDP ITE model, this may be encouraged by a 30° angle between tendon and bone components, incorporated into the design of molds, culture well inserts or bioreactors in conjunction with the trapezoidal interface.

Surgically, the angle of FDP fixation onto the DP varies with repair technique. Considering the most common techniques, in the standard pull-out button repair, sutures holding the tendon are drawn through an oblique anterograde DP drill hole for tying over the nailplate, whereas bone anchors holding the tendon are typically placed retrograde into the DP at 45°. Both aim to achieve secure tendon-bone contact, however it is unknown whether different insertion angles impact upon the direction of inserting tendon fibres once the healing attachment has matured and collagen fibres have realigned. From an anatomical standpoint, encouraging a 30° (anterograde) insertion of tendon fibres is optimal, most relevant to consider for drill angle when creating passage through the DP for the pull-out button repair sutures, as long as nailplate exit distal to the germinal matrix and lunula is maintained. Selection of bone anchor angle is primarily related to pull-out strength and avoidance of cortical penetration, however, although retrograde placement is classically viewed as the most biomechanically favourable,[43] anterograde angles have also been shown to give the same or greater load to failure,[44,45] possibly reflecting the more native insertion angle.

The limitations of this study are primarily related to the sample and measurement methodologies. Results aimed to provide population data descriptions, but were taken from a local Scottish sample with an age range (65 - 95) most likely older than the average age of patients with FDP avulsion. Later age is associated with histopathological enthesis changes such as microtears and microdamage,[46] however the tendon fibre angle measurement methodology mitigated against this by analysing multiple enthesis regions and excluding degenerated areas. The shape and size of the FDP enthesis is unlikely to change over time in healthy individuals, with results translatable to younger populations, but size variation may exist due to local genetics or other variables unknown to this sample such as height, body mass index or cumulative manual activity level. Sample size was determined through similar

and improved numbers from other cadaveric FDP insertion studies,[29,47] and although many significant differences were found across sex and finger groups in the limited sample, data interpretation has deliberately focused on the larger differences or recurring trends.

The measurement methodologies used were subjective, but were based on published techniques[25,29,35] and ICCs for all but 1 data set showed 'excellent' or 'good' reliability.[48] Apex width of the FDP footprint was the least reliable measurement, suggesting subjective rounding to the apex of the trapezoidal shape where determination of a horizontal measurement was difficult. Apex width measurements were small (range 1.33 - 2.11mm) and reliability of internal angle trapezoid measurements was excellent (ICC 0.99), implying that inter-observer variability was unlikely to impact meaningfully on trapezoid dimensions. However it is acknowledged that morphometrics, including tendon fibre angle, were linear measurements describing imperfectly straight lines, but were applied to extract useful, relatable data. Measurements were also 2-D representations of 3-D structures. Although the FDP footprint has a relatively flat profile for analysis, histological analysis was only undertaken in mid-sagittal section. Results from para-sagittal planes may have varied, however mid-sagittal was expected to be the optimal analysis plane since the central enthesis region contains the most organised collagen fibres[49] and most complex arrangement of fibrocartilaginous layers.[50]

4. CONCLUSION

In summary, this study his examined the native macroscopic and microscopic anatomy of the FDP enthesis, to gain greater morphological and biomechanical understanding of an important and commonly injured tendon-bone interface that may benefit from enhanced or novel treatments. The findings are distilled as potential recommendations to hand surgeons

and guides to interfacial tissue engineers for recreating the native insertion, and highlight region specific anatomical knowledge as the key to establishing translatable ITE models. These investigations may be applied to entheses in any body region, similarly providing the foundation to develop superior therapeutic options for a wide range of debilitating musculoskeletal injuries.

Abbreviations

FDP; Flexor digitorum profundus

DP: distal phalanx

5.DECLARATIONS

Ethics approval and consent to participate

Human cadaveric tissue was obtained from The University of Edinburgh Medical School body donation programme via written consent from all donors prior to death. All procedures and methods were regulated by The Human Tissue (Scotland) Act (2006) and no further ethical approval was required. All donor material used was from individuals who consented to photography before death and procedures were followed in accordance with local University of Edinburgh guidelines, set out by The Human Tissue (Scotland) Act (2006). .

Consent for publication

All donors consented to photography before death.

Availability of data and material

The datasets used and/or analysed during the current study are available from the corresponding author on reasonable request.

6. REFERENCES

1. Tuttle HG, Olvey SP, Stern PJ. 2006. Tendon avulsion injuries of the distal phalanx. Clin Orthop Relat Res 445: 157-168.

1   2. Ruchelsman DE, Christoforou D, Wasserman B, et al. 2011. Avulsion injuries of the flexor

2   digitorum profundus tendon. J Am Acad Orthop Surg 19(3): 152-162.

3   3. Boyes JH, Wilson JN, Smith JW. 1960. Flexor-tendon ruptures in the forearm and hand. J

4   Bone Joint Surg Am 42-A: 637-646.

5   4. Imbriglia JE, Goldstein SA. 1987. Intratendinous ruptures of the flexor digitorum

6   profundus tendon of the small finger. J Hand Surg Am 12(6): 985-991.

7   5. Freilich AM. 2015. Evaluation and treatment of jersey finger and pulley injuries in

8   athletes. Clin Sports Med 34(1): 151-166.

9   6. Rosberg HE, Carlsson KS, Dahlin LB. 2005. Prospective study of patients with injuries to

10   the hand and forearm: costs, function, and general health. Scand J Plast Reconstr Surg Hand

11   Surg 39(6): 360-369.

12   7. Dias JJ, Garcia-Elias M. 2006. Hand injury costs. Injury 37(11): 1071-1077.

13   8. Huq S, George S, Boyce DE. 2013. Zone 1 flexor tendon injuries: a review of the current

14   treatment options for acute injuries. J Plast Reconstr Aesthet Surg 66(8): 1023-1031.

15   9. Moiemen NS, Elliot D. 2000. Primary flexor tendon repair in zone 1. J Hand Surg Br

16   25(1): 78-84.

17   10. Tempelaere C, Brun M, Doursounian L, Feron JM. 2017. Traumatic avulsion of the flexor

18   digitorum profundus tendon. Jersey finger, a 29 cases report. Hand Surg Rehabil 36(5): 368-

19   372.

20   11. Benjamin M, Kumai T, Milz S, et al. 2002. The skeletal attachment of tendons—tendon

21   "entheses". Comp Biochem Physiol A Mol Integr Physiol 133(4): 931-945.

12. Benjamin M, Toumi H, Ralphs JR, et al. 2006. Where tendons and ligaments meet bone: attachment sites ('entheses') in relation to exercise and/or mechanical load. J Anat 208(4): 471-490.

13. Shaw HM, Benjamin M. 2007. Structure-function relationships of entheses in relation to mechanical load and exercise. Scand J Med Sci Sports 17(4): 303-315.

14. Schlecht SH. 2012. Understanding entheses: bridging the gap between clinical and anthropological perspectives. Anat Rec 295: 1239–1251.

15. Doschak MR, Zernicke RF. 2005. Structure, function and adaptation of bone-tendon and bone-ligament complexes. J Musculoskelet Neuronal Interact 5(1): 35-40.

16. Lu HH, Thomopoulos S. 2013. Functional attachment of soft tissues to bone: development, healing, and tissue engineering. Annu Rev Biomed Eng 15: 201-226.

17. Cooper RR, Misol S. 1970. Tendon and ligament insertion. A light and electron microscopic study. J Bone Joint Surg Am 52(1): 1-20.

18. Benjamin M, Ralphs JR. 1998. Fibrocartilage in tendons and ligaments — an adaptation to compressive load. J Anat 193(Pt 4): 481–494.

19. Apostolakos J, Durant TJ, Dwyer CR, et al. 2014. The enthesis: a review of the tendon-to-bone insertion. Muscles Ligaments Tendons J 4(3): 333-342.

20. Rodeo SA, Arnoczky SP, Torzilli PA, et al. 1993. Tendon-healing in a bone tunnel. A biomechanical and histological study in the dog. J Bone Joint Surg Am 75(12): 1795-1803.

21. Liu SH, Panossian V, al-Shaikh R, et al. 1997. Morphology and matrix composition during early tendon to bone healing. Clin Orthop Relat Res 339: 253-260.

22. Galatz LM, Sandell LJ, Rothermich SY, et al. 2006. Characteristics of the rat supraspinatus tendon during tendon-to-bone healing after acute injury. J Orthop Res 24(3): 541-550.

23. Silva MJ, Thomopoulos S, Kusano N, et al. 2006. Early healing of flexor tendon insertion site injuries: Tunnel repair is mechanically and histologically inferior to surface repair in a canine model. J Orthop Res 24(5): 990-1000.

24. Thomopoulos S, Williams GR, Soslowsky LJ. 2003. Tendon to bone healing: differences in biomechanical, structural, and compositional properties due to a range of activity levels. J Biomech Eng 125(1): 106-113.

25. Beaulieu ML, Carey GE, Schlecht SH, et al. 2015. Quantitative comparison of the microscopic anatomy of the human ACL femoral and tibial entheses. J Orthop Res 33(12): 1811-1817.

26. Evans EJ, Benjamin M, Pemberton DJ. 1990. Fibrocartilage in the attachment zones of the quadriceps tendon and patellar ligament of man. J Anat 171: 155-162.

27. Benjamin M, Evans EJ, Rao RD, et al. 1991. Quantitative differences in the histology of the attachment zones of the meniscal horns in the knee joint of man. J Anat 177: 127-134.

28. Benjamin M, Ralphs JR. 1995. Functional and developmental anatomy of tendons and ligaments. In: Gordon SL, Blair SJ, Fine LJ, editors. Repetitive motion disorders of the upper extremity. Rosemont, IL: American Academy of Orthopaedic Surgeons; p 185-203.

29. Chepla KJ, Goitz RJ, Fowler JR. 2015. Anatomy of the flexor digitorum profundus insertion. J Hand Surg Am 40(2): 240-244.

30. Leversedge FJ, Ditsios K, Goldfarb CA, et al. 2002. Vascular anatomy of the human flexor digitorum profundus tendon insertion. J Hand Surg Am 27(5): 806-812.

31. Benjamin M, Redman S, Milz S, et al. 2004a. Adipose tissue at entheses: the rheumatological implications of its distribution. A potential site of pain and stress dissipation? Ann Rheum Dis 63(12): 1549-1555.

32. Benjamin M, Moriggl B, Brenner E, et al. 2004b. The "enthesis organ" concept: why enthesopathies may not present as focal insertional disorders. Arthritis Rheum 50(10): 3306-3313.

33. Benjamin M, McGonagle D. 2007. Histopathologic changes at "synovio-entheseal complexes" suggesting a novel mechanism for synovitis in osteoarthritis and spondylarthritis. Arthritis Rheum 56(11): 3601-3609.

34. Benjamin M, Toumi H, Suzuki D, et al. 2007. Microdamage and altered vascularity at the enthesis-bone interface provides an anatomic explanation for bone involvement in the HLA-B27-associated spondylarthritides and allied disorders. Arthritis Rheum 56(1): 224-233.

35. Beaulieu ML, Carey GE, Schlecht SH, et al. 2016. On the heterogeneity of the femoral enthesis of the human ACL: microscopic anatomy and clinical implications. J Exp Orthop 3(1): 14.

36. Lee SK, Fajardo M, Kardashian G, et al. 2011. Repair of flexor digitorum profundus to distal phalanx: a biomechanical evaluation of four techniques. J Hand Surg Am 36(10): 1604-1609.

37. Benjamin M, Evans EJ, Copp L. 1986. The histology of tendon attachments to bone in man. J Anat 149: 89-100.

38. Redler I, Mow VC, Zimny ML, Mansell J. 1975. The ultrastructure and biomechanical significance of the tidemark of articular cartilage. Clin Orthop Relat Res 112: 357-362.

39. Frowen P, Benjamin M. 1995. Variations in the quality of uncalcified fibrocartilage at the insertions of the extrinsic calf muscles in the foot. J Anat 186(Pt 2): 417-421.

1   40. Benjamin M, Ralphs JR. 2004. Biology of fibrocartilage cells. Int Rev Cytol 233: 1-45.

2   41. Paxton, JZ, Baar K, Grover LM. 2012. Current progress in enthesis repair: strategies for

3   interfacial tissue engineering. Orthopedic Muscul Sys S1: 003.

4   42. Rothrauff BB, Tuan RS. 2014. Cellular therapy in bone-tendon interface regeneration.

5   Organogenesis 10(1): 13-28.

6   43. Burkhart SS. 1995. The deadman theory of suture anchors: observations along a south

7   Texas fence line. Arthroscopy 11(1): 119-123.

8   44. Schreuder FB, Scougall PJ, Puchert E, et al. 2006. The effect of mitek anchor insertion

9   angle to attachment of FDP avulsion injuries. J Hand Surg Br 31(3): 292-295.

10   45. Clevenger TA, Beebe MJ, Strauss EJ, Kubiak EN. 2014. The effect of insertion angle on

11   the pullout strength of threaded suture anchors: a validation of the deadman theory.

12   Arthroscopy 30(8): 900-905.

13   46. Villotte S, Knüsel CJ. 2013. Understanding entheseal changes: definition and life course

14   changes. Int J Osteoarchaeol 23: 135–146.

15   47. Bond S, Rust P, Boland M. 2019. The accommodation of bone anchors within the distal

16   phalanx for repair of flexor digitorum profundus avulsions. J Hand Surg Am 44(11): 986.e1-

17   986.e6.

18   48. Koo TK, Li MY. 2016. A guideline of selecting and reporting intraclass correlation

19   coefficients for reliability research. J Chiropr Med 15(2): 155-163.

20   49. Thomopoulos S, Marquez JP, Weinberger B, et al. 2006. Collagen fiber orientation at the

21   tendon to bone insertion and its influence on stress concentrations. J Biomech 39(10): 1842-

22   1851.

50. Milz S, Rufai A, Buettner A, et al. 2002. Three-dimensional reconstructions of the

Achilles tendon insertion in man. J Anat 200(2): 145–152.

FIGURE LEGENDS

Figure 1. FDP Footprint Generation

a) Excised distal phalanx (*DP*) bone with attached FDP tendon (flexor surface). **b)** Tendon-

bone sample after methylene blue immersion. **c)** DP after sharp excision of the FDP at

insertion, leaving the unstained *FDP footprint*. **d)** Binary mask image of the FDP footprint for

morphometric analysis.

Figure 2. Tendon Fibre Angle Measurement Methodology

a) *Inset*: Side view of an example pre-sectioned tendon(*T*)-bone(*B*) sample [ungual tuberosity

removed from the distal bone end (*left* side of image)], with box showing enthesis region of

main panel. *Main panel*: The tidemark (*superimposed line*) is traced along the length of the

FDP enthesis, from proximal (*right*) to distal (*left*). **b)** A line of best fit of the tidemark is

produced, marking the points at *20%, 40%, 50%, 60%* and *80%* along the enthesis. **c)**

Example measurements of angle of tidemark intersection fibres (α) and angle of approaching

fibres (β) at 20% along the enthesis. The location of 20% along the tidemark is found on a

perpendicular line (*broken line*) from 20% along the line of best fit of the tidemark (*dotted

line*). The angle of tidemark intersection (α) measures the angle of directly intersecting fibres;

the angle of approach (β) measures a line parallel to the average angle of fibres approaching

over a preceding 20% distance of the enthesis. Angles are measured against a line parallel to

the line of best fit of the tidemark (*dotted line*). **d)** Magnified view to highlight the angle of

tidemark (*TM*) intersection (α) at this 20% enthesis measurement point. Mid-sagittal section

micrographs of an FDP enthesis, toluidine blue. *CB* - cortical bone; *TB* - trabecular bone.

1   **Figure 3. FDP Footprint Shape and Size**

2   Complete set of unstained FDP footprints on stained DPs, with each binary 'mask' footprint

3   below, showing trapezoidal footprint shape. Scale bars 2mm. **b)** Comparison of footprint

4   trapezoid left and right internal angles. Non-significant (*ns*) differences suggest a

5   symmetrical shape across the vertical axis. **c)** Footprint surface area, compared within sex

6   and finger categories. The little finger is the principle source of significant size differences.

7   Mean ± standard error. *p<0.05, **p<0.01, ***p<0.001.

8

9   **Figure 4. The Fibrocartilaginous FDP Enthesis**

10   The FDP insertion demonstrates the 4 zones of a fibrocartilaginous enthesis: tendon (*T*),

11   uncalcified fibrocartilage (*UF*), calcified fibrocartilage (*CF*) and bone. The cortical bone

12   (*CB*) is as thin as the trabecular bone (*TB*). The calcified fibrocartilage lies between the

13   tidemark (*black arrows*) and the tendon-bone junction (*grey arrows*). Fibrochondrocytes

14   (*white arrows*), rounded and lying in lacunae within cartilage matrix, indicate cartilaginous

15   areas and generally align in rows. Tendon collagen fibre bundles are continuous through the

16   fibrocartilage areas to attach to the cortical bone. Photomicrograph of a typical mid-sagittal

17   section FDP enthesis, H+E.

18

19   **Figure 5. FDP Enthesis Regional Variation**

20   Entire sample section (proximal – *right*; distal – *left*), showing FDP tendon (*T*) attachment; *b*,

21   *c* and *d* indicate subsequent panel regions **b)** Proximal enthesis region. The 4

22   fibrocartilaginous enthesis zones are apparent. The approaching tendon fibres undergo a

23   considerable angle change in reaching the tidemark (*TM*) and cortical bone (*CB*). The

24   majority of the angle change occurs in the uncalcified fibrocartilage (*UF*) zone, demonstrated

25   by the curved columns of fibrochondrocytes (*white arrows*), with straight tendon fibres in the

calcified fibrocartilage (*CF*) zone. **c)** Middle enthesis region. A calcified fibrocartilage (*CF*)

zone is present, although less thick than in the proximal region, with a variable layer of

uncalcified fibrocartilage (*UF*) demonstrated by the limited but perceptible fibrochondrocytes

(*white arrow*). Compared to the proximal enthesis region, the approaching tendon fibres are

generally less acute to the horizontal, and there is less angle change between the approaching

fibres and tidemark intersection fibres. **d)** Distal enthesis region. Areas of calcified

fibrocartilage (*CF*) are sporadic and are interspersed between fibrous enthesis regions which

lack any fibrocartilage. The absence of fibrochondrocytes proximal to the calcified

fibrocartilage indicates no uncalcified fibrocartilage zone. Tendon fibres approach the

tidemark (*TM*) more acutely than the middle enthesis region. Micrographs of a typical mid-

sagittal section of an FDP enthesis, toluidine blue (**a-d**). e) Quantified angle change

comparison between the 5 distance measurement points along the thesis. Mean ± standard

error **p<0.01, ***p<0.001.

Figure S1. FDP Footprint Image Analysis

a) Lower half of stained DP with unstained FDP footprint. *Dotted line* shows mapped FDP footprint

perimeter, *full line* shows consequent bounding box, processed to create the binary mask footprint

image within its bounding box [(**b**) and (**c**)]. Footprint surface area is quantified from the area inside

the footprint perimeter. **b)** General footprint measurements. Base width (*BW*) is the widest

measurement (i.e. width of bounding box), and apex width (*AW*) is the highest point at which the

sloping sides turn horizontally towards the midline. Height is calculated as the mean of height at mid-

width of the bounding box (H_1) and maximum height (H_2, i.e. height of bounding box). **c)** 4 internal

angles (apex left, *AL*; apex right, *AR*; base left, *BL*; base right, *BR*) are calculated as a mean of 2

trapezoids (subscripts *1* and *2)*. The base of the trapezoids are defined by the perpendicular at the

highest point of left or right bounding box intersection (subscript *1*, *dotted line*) or at the lowest point

of the footprint (subscript *2*, *broken line*). Apices are positioned the same for both trapezoids.

1   **Table 1.** FDP Footprint Morphometrics (mm). Results presented as Mean (± standard error).

2

3   **Table 2.** Angle (º) of Inserting Fibres Averaged Across All Distance Measurement Points.

4   Results presented as Mean (± standard error).

5

6   **Table 3.** 3-Level Size Guide Dimensions (mm) for Trapezoidal FDP Insertion.

7   *Large*: male index, middle, ring finger. *Medium*: male little finger; female index, middle,

8   ring finger. *Small*: female little finger.

9

10

11

12

13

14

15

16

17

18

19

20

21

22

23

24

25

26

27

28

29

30

31

1   **ADDITIONAL FILES**

2   **Figure S1**

3   **FDP Footprint Image Analysis**

4   This figure shows how specific aspects of the FDP footprint were measured and calculated.

5

6   **Table S-1.**

7   Internal Angles (º) of FDP Footprint Trapezoid

8   Results are presented as Mean (± standard error).

9

10   **Table S-2.**

11   Angle (º) of Inserting Fibres at Enthesis Distance Measurement Points

12

13

14   **Table S-3.**

15   Angle (º) of Approaching Fibres at Enthesis Distance Measurement Points

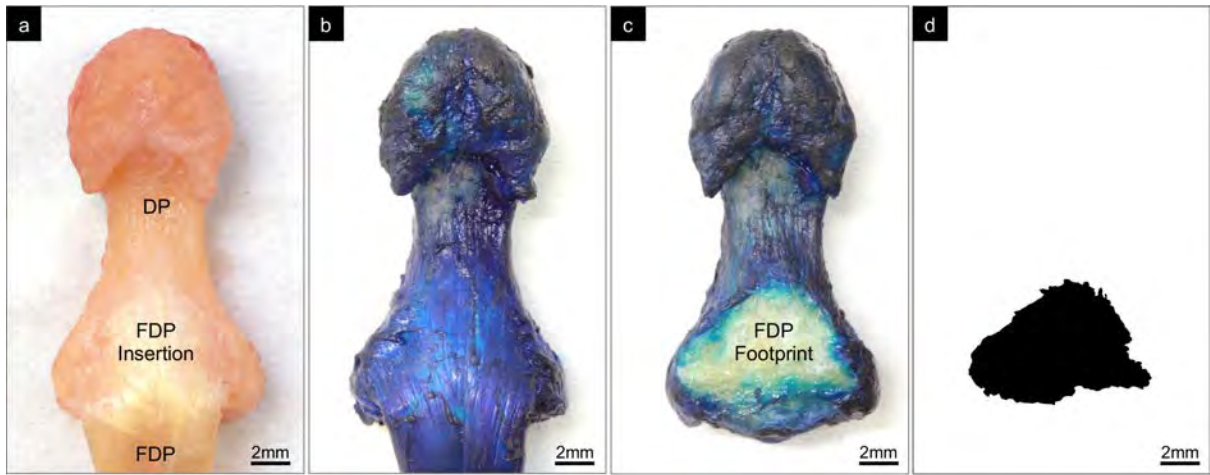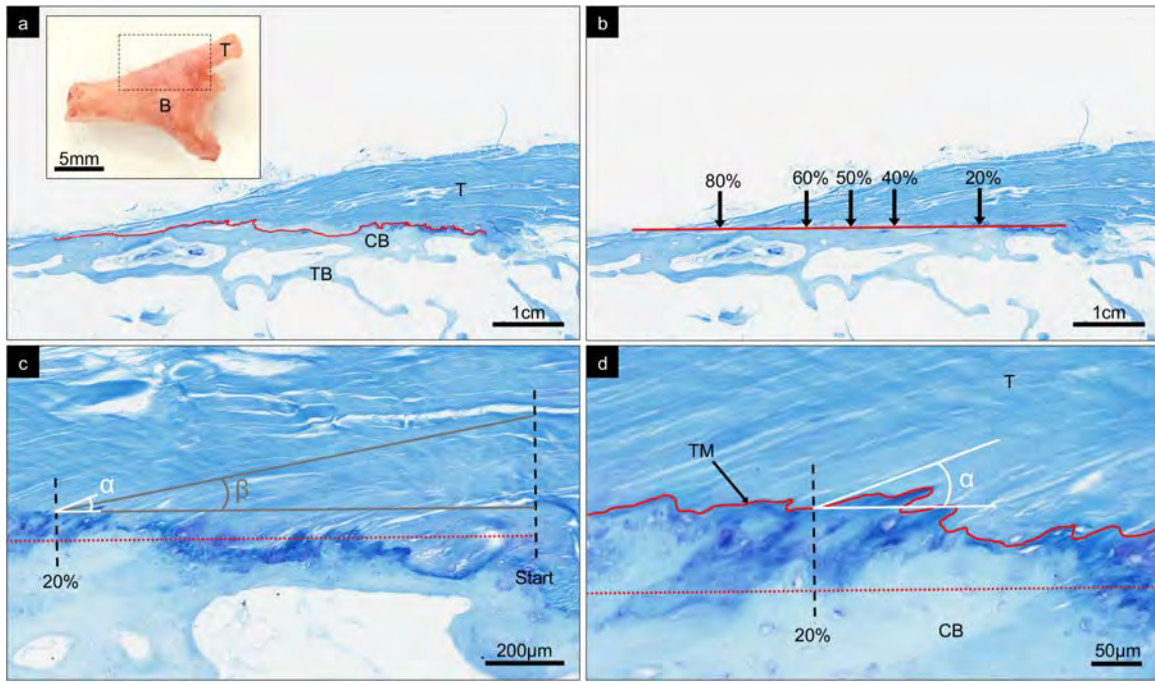16   Results are presented as Mean (± standard error).

17

18

19

20

21

22

23

24

Figure 1.

Figure 2
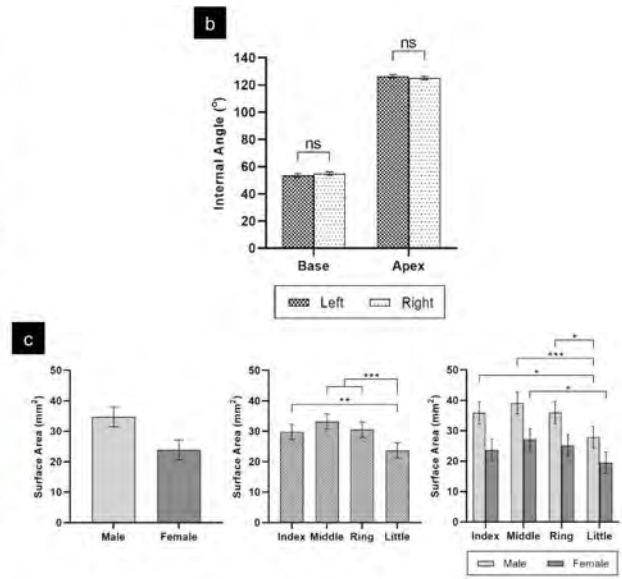
1

2   Figure 3

3

4

5

6

7

8

9

Figure 4

Figure 5

Figure S1

1 **Table 1.** FDP Footprint Morphometrics (mm)
2

Finger	Height			Base Width			Apex Width		
	Male	**Female**	*All*	**Male**	**Female**	*All*	**Male**	**Female**	*All*
Index	6.51 (0.34)	4.95 (0.34)	5.73 (0.24)	9.04 (0.56)	7.79 (0.56)	8.41 (0.40)	1.72 (0.27)	1.44 (0.27)	1.58 (0.20)
Middle	6.59 (0.34)	4.86 (0.34)	5.73 (0.24)	9.77 (0.56)	8.62 (0.56)	9.20 (0.40)	1.42 (0.27)	2.11 (0.27)	1.77 (0.20)
Ring	6.24 (0.36)	4.97 (0.34)	5.61 (0.25)	9.44 (0.58)	8.11 (0.56)	8.77 (0.40)	1.83 (0.29)	1.33 (0.27)	1.56 (0.20)
Little	5.20 (0.34)	4.23 (0.34)	4.72 (0.24)	8.46 (0.56)	7.46 (0.56)	7.96 (0.40)	1.37 (0.27)	1.66 (0.27)	1.52 (0.20)
All	6.14 (0.30)	4.75 (0.29)	5.45 (0.21)	9.18 (0.52)	7.99 (0.52)	8.58 (0.37)	1.57 (0.16)	1.63 (0.15)	1.60 (0.11)

3
4 Mean (± standard error).
5

6 **Table 2.** Angle (º) of Inserting Fibres Averaged Across All Distance Measurement Points
7

Finger	Male	Female	*All*
Index	26.77 (1.85)	33.96 (1.85)	30.37 (1.30)
Middle	27.98 (2.03)	31.37 (1.85)	29.62 (1.35)
Ring	28.42 (1.85)	31.51 (1.85)	29.96 (1.30)
Little	28.07 (1.85)	32.44 (2.03)	30.26 (1.35)
All	27.78 (1.01)	32.33 (1.01)	30.05 (0.72)

8
9 Mean (± standard error).
10

11 **Table 3.** 3-Level Size Guide Dimensions (mm) for Trapezoidal FDP Insertion
12

Size	Height	Base Width	Apex Width
Large	6	9	2
Medium	5	8	2
Small	4	7	2

13
14 *Large*: male index, middle, ring finger. *Medium*: male little finger; female index, middle, ring
15 finger. *Small*: female little finger.
16

17

18

1 **Table S-1.** Internal Angles (º) of FDP Footprint Trapezoid

2

Finger	Base		Apex	
	Left	Right	Left	Right
Male				
Index	57.88 (3.02)	60.02 (2.09)	122.14 (3.02)	119.91 (2.09)
Middle	56.50 (3.02)	53.86 (2.09)	123.49 (3.02)	126.14 (2.09)
Ring	54.50 (3.22)	55.02 (2.28)	125.51 (3.23)	124.96 (2.28)
Little	52.48 (3.02)	52.65 (2.09)	127.55 (3.02)	127.50 (2.09)
All	55.36 (2.17)	55.43 (1.22)	124.65 (2.17)	124.58 (1.22)
Female				
Index	54.60 (3.02)	55.32 (2.09)	125.38 (3.02)	124.70 (2.09)
Middle	50.18 (3.02)	52.95 (2.09)	129.83 (3.02)	127.08 (2.09)
Ring	51.69 (3.02)	55.79 (2.09)	128.29 (3.02)	124.17 (2.09)
Little	50.41 (3.02)	53.56 (2.09)	129.62 (3.02)	126.53 (2.09)
All	51.72 (2.15)	54.41 (1.20)	128.28 (2.15)	125.62 (1.21)
Collective				
All	53.54 (1.53)	54.92 (0.85)	126.47 (1.53)	125.10 (0.86)

3

4 Mean (± standard error).

5

6 **Table S-2.** Angle (º) of Inserting Fibres at Enthesis Distance Measurement Points

7

Finger	20%			40%			50%		
	Male	**Female**	*All*	**Male**	**Female**	*All*	**Male**	**Female**	*All*
Index	28.08 (5.15)	43.60 (5.95)	34.53 (3.96)	26.97 (3.20)	36.14 (3.20)	31.56 (2.17)	28.70 (3.85)	29.27 (4.30)	29.08 (2.74)
Middle	29.08 (5.42)	36.67 (4.95)	32.96 (3.72)	34.56 (4.53)	39.43 (5.55)	37.16 (3.37)	26.44 (4.97)	29.55 (4.30)	28.05 (3.11)
Ring	27.61 (5.79)	31.65 (4.95)	29.23 (3.82)	30.99 (3.92)	36.83 (4.53)	33.96 (2.85)	30.07 (3.85)	31.18 (3.85)	30.63 (2.59)
Little	30.32 (4.95)	26.80 (6.63)	31.16 (3.97)	27.01 (3.20)	28.20 (7.84)	29.52 (3.02)	28.75 (3.85)	34.66 (6.09)	30.93 (3.16)
All	28.77 (4.36)	35.18 (4.42)	31.97 (3.09)	29.77 (1.77)	36.33 (2.31)	33.05 (1.47)	28.54 (1.96)	30.80 (2.16)	29.67 (1.45)
Finger	60%			80%					
	Male	**Female**	*All*	**Male**	**Female**	*All*			
Index	25.25 (3.12)	28.49 (3.12)	26.87 (2.27)	22.42 (4.02)	32.95 (3.60)	28.04 (2.65)			

Middle	25.58 (2.79)	25.45 (2.79)	25.51 (2.03)	30.39 (4.02)	30.38 (3.29)	29.97 (2.52)
Ring	25.10 (2.79)	31.61 (2.79)	28.35 (2.03)	26.14 (3.60)	28.56 (3.29)	27.27 (2.39)
Little	29.34 (2.79)	42.17 (3.60)	34.81 (2.29)	22.95 (8.05)	27.67 (4.65)	25.46 (4.03)
All	26.27 (1.48)	31.50 (1.57)	28.89 (1.08)	25.62 (2.26)	29.75 (1.83)	27.69 (1.51)

Mean (± standard error).

Table S-3. Angle (º) of Approaching Fibres at Enthesis Distance Measurement Points

Finger	20%			40%			50%		
	Male	**Female**	*All*	**Male**	**Female**	*All*	**Male**	**Female**	*All*
Index	14.21 (3.34)	13.85 (4.01)	14.52 (2.60)	16.56 (2.63)	18.35 (2.63)	17.48 (1.79)	15.52 (2.06)	19.60 (2.22)	17.56 (1.44)
Middle	9.86 (3.66)	10.65 (3.34)	10.13 (2.53)	14.85 (2.97)	17.57 (2.78)	16.08 (1.96)	11.89 (2.80)	18.79 (2.22)	15.82 (1.67)
Ring	4.87 (4.48)	11.06 (3.34)	9.03 (2.67)	14.31 (2.97)	21.52 (3.04)	17.86 (2.06)	15.68 (2.06)	17.59 (2.22)	16.73 (1.44)
Little	10.02 (3.34)	12.90 (3.66)	11.41 (2.53)	13.61 (2.63)	19.63 (3.23)	16.29 (1.96)	18.06 (2.22)	21.05 (2.48)	19.56 (1.58)
All	10.21 (3.07)	12.34 (3.06)	11.27 (2.16)	14.90 (2.01)	18.95 (2.05)	16.92 (1.43)	15.55 (1.30)	19.28 (1.30)	17.42 (0.92)
Finger	60%			80%			Average		
	Male	**Female**	*All*	**Male**	**Female**	*All*	**Male**	**Female**	*All*
Index	14.48 (1.85)	16.96 (1.85)	15.71 (1.33)	12.45 (2.44)	13.25 (2.24)	12.85 (1.63)	14.93 (1.73)	16.86 (1.73)	15.89 (1.21)
Middle	11.06 (1.85)	16.84 (1.85)	13.92 (1.33)	15.45 (2.44)	13.61 (2.10)	14.30 (1.57)	12.08 (1.82)	15.10 (1.73)	13.64 (1.24)
Ring	16.22 (1.85)	14.92 (1.85)	15.57 (1.33)	13.86 (2.24)	16.27 (2.10)	15.18 (1.52)	14.65 (1.73)	15.66 (1.73)	15.16 (1.21)
Little	20.30 (1.74)	20.01 (1.85)	20.25 (1.38)	13.92 (2.24)	13.41 (2.10)	13.62 (1.52)	14.88 (1.73)	17.31 (1.73)	16.10 (1.21)
All	15.56 (1.31)	17.17 (1.32)	16.36 (0.93)	13.86 (1.57)	14.12 (1.51)	13.99 (1.09)	14.16 (1.38)	16.23 (1.37)	15.20 (0.97)

Mean (± standard error).